Comparison of Pulsed Sinusoid Radio Frequency Interference Detection Algorithms Using Time and Frequency Sub-Sampling

Sidharth Misra and Christopher Ruf
Department of Atmospheric, Oceanic and Space Sciences
University of Michigan
2455 Hayward St., Ann Arbor, MI, 48109-2143 USA

***Abstract*— The performance of two major Radio Frequency Interference (RFI) detection algorithms is compared. The peak detection algorithm and the kurtosis detection algorithm are characterized using the receiver operating characteristic (ROC) for pulsed sinusoid RFI. Downlink data bandwidth is one of the major design factors to be considered when comparing detection algorithms. Results are presented in this paper that compare the kurtosis algorithm performance with an ideally matched peak detection algorithm. The RFI parameters are also varied to analyze the overall detection performance of both algorithms. Factors such as implementation details, resource usage, post-processing and practicality are also addressed for both algorithms.**

***Index terms* – Microwave radiometry, radio frequency interference**

I. Introduction

Extremely pervasive levels of Radio Frequency Interference (RFI) have been observed by a number of spaceborne microwave radiometers in their C- and X-Band channels [1-5]. As a result, a number of RFI detection and mitigation approaches have been developed, using both hardware and software means. These approaches to detection can be generally divided into two classes: "Peak detection" compares the power in samples of the signal (*i.e.* its 2nd central moment) to expected power levels and considers anomalously high values to be caused by RFI [6]. "Kurtosis detection" evaluates the 4th central moment of a signal divided by the square of its 2nd central moment and considers as RFI those values which differ from that of a Gaussian distributed signal [7].

Peak detection uses a conventional square-law detector whereas kurtosis detection requires specialized detector hardware/firmware. RFI mitigation can be accomplished by dividing a sample into temporal subsamples and removing only the contaminated ones, dividing a sample into spectral subsamples and removing only the contaminated ones, or both. Any of these three mitigation approaches can be used with either of the two approaches to detection [7-11].

RFI is often localized in time and frequency, relative to the integration times and pre-detection bandwidths over which a spaceborne microwave radiometer acquires its samples of brightness temperature. As a result, the number of subsamples –in both time and frequency– into which a sample is divided can affect the detectability of the RFI. In general, the more closely matched the subsample time and frequency intervals are to the characteristics of the RFI, the better the detection. However, such matching often requires fairly finely resolved subsamples. Finely resolved temporal subsamples can drive up the data rate of a radiometer. Finely resolved spectral samples can increase both the data rate and the real time signal processing requirements (and, hence, the power). The work presented here addresses the cost/benefit trade-off between the data bandwidth and the quality of RFI detection and mitigation performance as a function of the detection algorithm.

In Section II, we give a brief background of the peak detection algorithm. Section III introduces the kurtosis detection algorithm. The performance of the two detection algorithms is compared and relevant results are presented in Section IV.

II. Peak Detection Algorithm

The peak detection algorithm works on a simple threshold principle. The thermal emission signal measured by the radiometer is digitized (assuming a digital detector) and the resulting samples are squared. These squared samples are then integrated over a sub-sample time period to determine the time-averaged power. If that power is above a certain threshold value then the sub-sample is flagged as containing RFI. The threshold value is determined from the mean and standard deviation of the data itself.

Typically, in order to successfully identify and remove RFI the sub-sample integration period should be orders of magnitude smaller than the nominal integration time of the radiometer's science data products, and it should be closely matched with the duration of the RFI itself.

A radiometer signal is generated by thermal emission and its amplitude is random in nature with a Gaussian distribution. As a result its squared samples follow a Chi-square distribution. The false-alarm rate (FAR), shown in Eqn. 1, of the detection algorithm for a single sub-sample can easily be calculated using the right tail distribution [12]

This work was supported in part by NASA Grant NNG04HZ28C.

$$Q_{\chi^2_N}(z) = e^{-\frac{1}{2}z} \sum_{k=0}^{\frac{N}{2}-1} \frac{\left(\frac{x}{2}\right)^k}{k!} \quad (1)$$

where z is the threshold value and N is the number of samples used within one integration period, thus indicating a FAR calculated for a Chi-Square distribution with N degrees of freedom. Eqn. 1 can easily be extended to find FAR for detection with multiple sub-samples within an integration period.

III. Kurtosis Detection Algorithm

Radiometric sources include natural thermal emission from the scene as well as thermal noise generated by the sensor. The kurtosis detection algorithm takes advantage of the randomness of the incoming signal. The probability distribution function of a radiometric source signal is Gaussian in nature, whereas man-made RFI sources generally have a non-Gaussian distribution [7]. The kurtosis algorithm measures the deviation of the incoming signal from normality to check for the presence of interfering sources.

The detection algorithm measures the ratio of the 4th central moment to the square of the 2nd central moment, also known as the kurtosis, as shown in equation 2. The second central moment is similar to the power measurements made in the peak detection algorithm.

$$\kappa = \frac{m_4}{m_2^2} \quad (2)$$

where $m_n = \langle (x - \langle x \rangle)^n \rangle$ is the n^{th} central moment, x(t) is the signal and $\langle\ \rangle$ is the expectation operator. If the incoming signal is purely Gaussian then the kurtosis ratio equals three. If there is a non-normal interfering signal present then the kurtosis will deviate from three. The value of the kurtosis is independent of variations in the brightness temperature of the scene being observed.

Since the kurtosis is generally calculated from a finite sample set, it itself behaves like a random variable [11]. Estimates of the kurtosis have a standard deviation associated with them and there is a corresponding kurtosis threshold for detecting RFI. For a sufficiently large sample size, the kurtosis statistic has a normal distribution and the FAR of the detection algorithm (assuming equal thresholds above and below the kurtosis mean) is given by,

$$Q_\kappa(z) = \left(1 - erf\left(\frac{z}{\sqrt{2}}\right)\right) \quad (3)$$

where z is the normalized standard deviation magnitude of the kurtosis, beyond which a sample is flagged as being corrupted by RFI.

In practical implementations of the detection algorithm the incoming signal is divided into temporal as well as spectral sub-samples before calculating the kurtosis statistic [7]. If any sub-sample is flagged then it is discarded. In order to compare the kurtosis algorithm with the peak detection algorithm, an entire integration period is assumed to be corrupted by RFI if any single sub-sample is flagged. Eqn. 3 can be rewritten to calculate the FAR for detection of the whole temporal/spectral grid of sub-samples within the integration period.

IV. Algorithm Comparison

A. *RFI model and ROC area parameter*

The performance of the two detection algorithms is compared with respect to a common pulsed-sinusoidal RFI source. The incoming radiometric signal can be written as,

$$x[n] = \begin{cases} a[n] & 1,..,m < n < m+d,..,M \\ a[n] + A\sin(2\pi f_o n) & ,else \end{cases} \quad (4)$$

where $a \sim N(\mu,\sigma)$, A is the amplitude of the pulsed-sinusoid signal with frequency f_o, and M is the total radiometer integration period. The duty cycle of the sinusoidal pulse is therefore given by d/M.

The two RFI parameters that can vary are its duty cycle and amplitude (or power). These parameters significantly affect the detection performance. The behavior of the kurtosis algorithm under pulsed-sinusoidal RFI has been extensively analyzed in [11]. The kurtosis algorithm is extremely sensitive at low duty cycles, and a blind-spot exists for sinusoidal RFI with 50% duty-cycle. This typically isn't a problem since most radar signals have a very low duty-cycle. The probability of detection (PD) for the kurtosis algorithm can be calculated if the duty-cycle and power of the RFI signal are known.

The peak detection algorithm performs best when the sub-sample integration time is matched to the pulse-width of the RFI. The performance degrades as that integration time increases relative to the pulse-width. Due to RFI, the probability distribution of power of the incoming thermal signal would be a non-central Chi-square distribution with the non-centrality parameter determined by the power and duty cycle of the RFI. The PD of the peak detection algorithm can be calculated for a particular RFI power and duty cycle using the pdf.

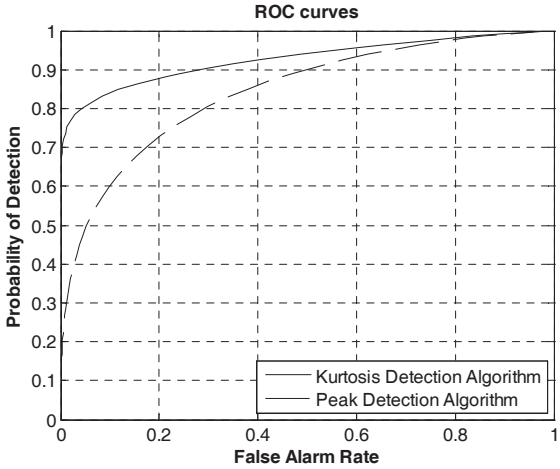

Fig 1: Plot indicating the ROC curves for two RFI detection algorithms for a 0.33% duty-cycle pulsed-sinusoid RFI with a 0.5NEΔT power level.

The ROC of any detection algorithm can be obtained from its FAR and PD. Fig. 1 indicates the ROC curves of the kurtosis algorithm and peak detection algorithm for RFI with a duty cycle of 0.33% and power of 0.5NEΔT. For Fig. 1, the kurtosis algorithm uses 16 subbands and has a sub-sampling period that is a quarter of the total integration period, whereas the peak detection algorithm divides the total integration period into 1200 sub-sampling periods. In general, better detection algorithms correspond to an ROC curve that is closer to the upper left corner of the PD vs. FAR space.

The normalized area under the ROC curve is used as a parameter to estimate the relative performance of the detection algorithms under various conditions. An ROC area of 1 indicates an ideal detector. In Fig. 1, the kurtosis algorithm for the given RFI power and duty cycle has an ROC area of 0.92, whereas the peak detection algorithm has an ROC area of 0.84. These values suggest that the kurtosis algorithm is the better algorithm for that particular type of RFI.

B. *ROC area comparison – Matched operating point*

The performance of the kurtosis detection algorithm is considered for pulsed sinusoid RFI whose pulse duration is perfectly matched to the sub-sample integration time of the peak detection algorithm. The digitizer is expected to operate at 240MHz, with a radiometer integration time of 1ms. The pulse width of RFI is assumed to be a typical value of 1.66μs for radar signals and the peak detection algorithm is nearly optimally matched with 200 raw samples in one sub-sample period.

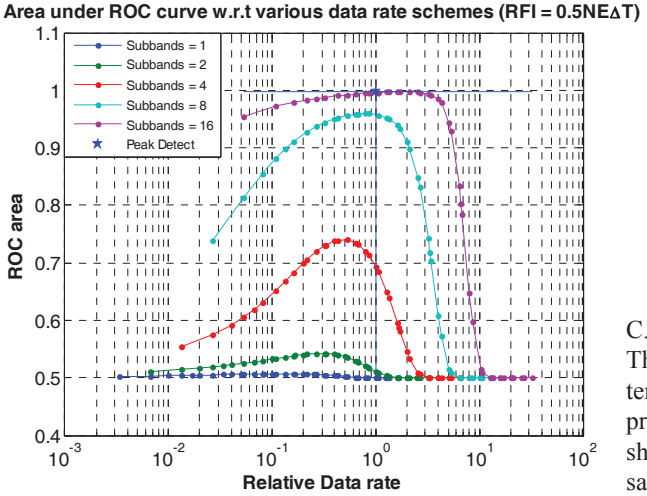

Fig 2: Plot comparing the ROC area for the kurtosis algorithm under various data rates schemes and subbands with the matched peak detection algorithm (star) (RFI power = 0.5NEΔT)

Fig. 2 compares the ROC area of the kurtosis algorithm with a matched peak detection algorithm for various data rates and numbers of sub-bands. The data-rate is an important factor when considering algorithm performance. Even though the peak detection performs extremely well when matched with the RFI pulse-width, the resulting data-rate due to such finely resolved sub-samples might be impractical in terms of downlink bandwidth. The peak detection algorithm just needs to send the power (2nd moment) of the incoming thermal emissions, whereas kurtosis needs to send the first four moments to calculate the kurtosis ratio. These four pieces of information are sent for each sub-band used by the kurtosis. The data rate of the kurtosis algorithm benefits from having a much longer sub-sample period compared to the peak detection algorithm.

As Fig. 2 indicates, for RFI power 0.5 times the NEΔT, the matched peak detection algorithm has an almost ideal performance (ROC area = 1). The kurtosis algorithm with 16 subbands has nearly comparable performance, with an ROC area of 0.9 or greater, and it has a significantly lower data-rate. The kurtosis detection algorithm performance suffers as its sub-sample period becomes shorter and the pulse-width approaches a 50% duty-cycle. Fig. 3 is similar to Fig. 2, except that the RFI power is 1.5 times the NEΔT. The peak detection algorithm still has near ideal performance. However, the kurtosis algorithm performs nearly as well as the peak detect algorithm with much lower relative data-rates.

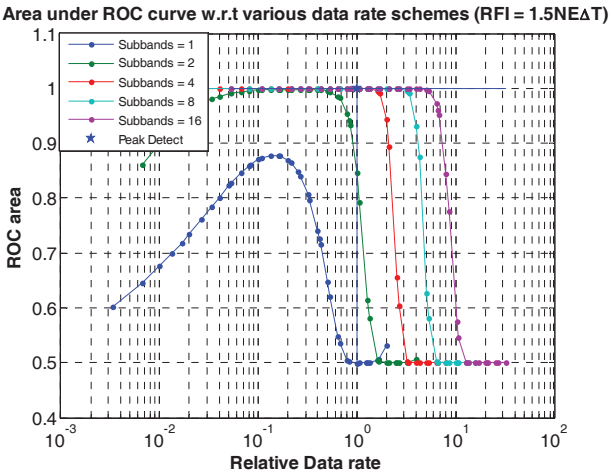

Fig 3: Plot comparing the ROC area for the kurtosis algorithm under various data rates schemes and subbands with the matched peak detection algorithm (star) (RFI power = 1.5NEΔT)

C. *ROC area difference – Multiple RFI conditions*

The optimum operating point for both detection algorithms in terms of sub-sample integration time depends on certain properties of the RFI. For the peak detection algorithm, it should equal the pulse width, which equates to 200 raw samples. For the kurtosis detection algorithm, 16 subbands and 60,000 raw samples yields peak performance, thus requiring a factor of four less data rate than the peak detection algorithm.

Fig. 4 indicates the difference in performance between the two detection algorithms in terms of ROC area with respect to different RFI power levels and duty-cycles. If the ROC area for both algorithms is below 0.75, then the detection performance is considered poor enough that the difference can be ignored.

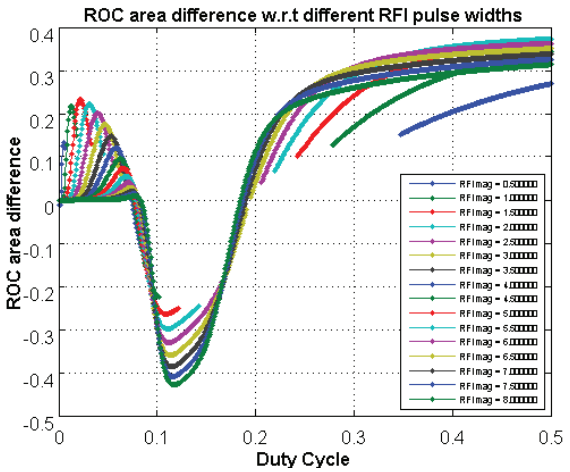

Fig 4: Plot indicating difference between ROC areas of the kurtosis detection algorithm and peak detection algorithm for different RFI pulse widths and duty cycles (60K accum. Samples)

In the above figure, a positive value indicates that the kurtosis algorithm performs better and a negative value indicates better peak detection algorithm performance. For low-power and low duty cycles the kurtosis algorithm is sensitive to RFI, whereas for higher duty cycle signals (continuous-wave) the performance of the peak detection algorithm degrades significantly as the power gets lower. The peak detection algorithm performs best when perfectly matched with the RFI, as seen extremely low duty cycles, though the difference is not large.

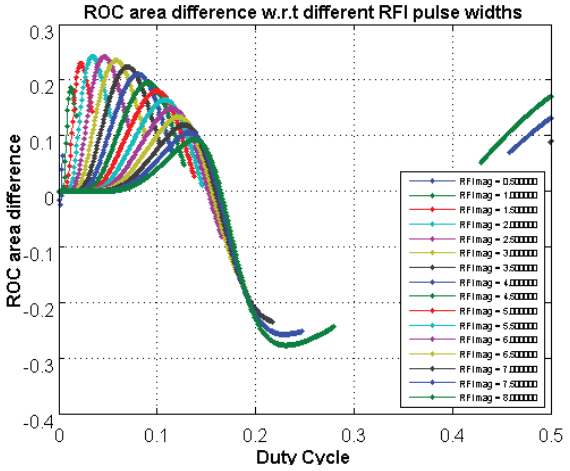

Fig 5: Plot indicating difference between ROC areas of the kurtosis detection algorithm and peak detection algorithm for different RFI pulse widths and duty cycles (120K accum. Samples)

The detection performance of the kurtosis algorithm can be improved by combining different accumulation periods and recalculating the kurtosis ratio in post-processing. The 50% duty cycle blind spot can be avoided by combining multiple sub-samples in ground processing. Fig. 5 indicates the ROC area difference when the kurtosis algorithm combines its 60,000 accumulation samples to 120,000 samples. As noted in the figure, the blind-spot present in Fig. 4 is easily removed in Fig. 5. The authors are currently working on methods of optimizing detection by taking advantage of combining accumulation periods.

V. Conclusion and Discussion

The peak detection algorithm and the kurtosis algorithm are two RFI mitigation and detection techniques developed for microwave remote sensing. The performance of both algorithms is characterized using the ROC area for pulsed-sinusoid type RFI. Results indicate that the peak detection algorithm has superior detectability when its sub-sample integration time matches the RFI pulse-width. The kurtosis algorithm can achieve nearly the same performance at a considerably lower data rate. The kurtosis algorithm with subbanding has superior detection performance for RFI with varying duty cycle and power.

References

[1] Li Li, E.G. Njoku, E. Im, P.S. Chang and K.S. Germain, "A preliminary survey of radio-frequency interference over the U.S. in Aqua AMSR-E data," Geoscience and Remote Sensing, IEEE Transactions on, vol. 42, pp. 380-390, 2004.
[2] E.G. Njoku, T.K. Chan, W. Crosson and A. Limaye, "Evaluation of the AMSR-E Data Calibration over Land," Rivista Italiana Di Telerilevamento - Italian Journal of Remote Sensing, vol. 30, pp. 15, 2004.
[3] E.G. Njoku, P. Ashcroft, T.K. Chan and Li Li, "Global survey and statistics of radio-frequency interference in AMSR-E land observations," Geoscience and Remote Sensing, IEEE Transactions on, vol. 43, pp. 938-947, 2005.
[4] L. Li, P.W. Gaiser, M.H. Bettenhausen and W. Johnston, "WindSat radio-frequency interference signature and its identification over land and ocean," Geoscience and Remote Sensing, IEEE Transactions on, vol. 44, pp. 530-539, 2006.
[5] S.W. Ellingson and J.T. Johnson, "A polarimetric survey of radio-frequency interference in C- and X-bands in the continental united states using WindSat radiometry," Geoscience and Remote Sensing, IEEE Transactions on, vol. 44, pp. 540-548, 2006.
[6] N. Niamsuwan, J.T. Johnson and S.W. Ellingson, "Examination of a simple pulse-blanking technique for radio frequency interference mitigation," Radio Science, vol. 40, pp. 11, 2005.
[7] C.S. Ruf, S.M. Gross and S. Misra, "RFI detection and mitigation for microwave radiometry with an agile digital detector," Geoscience and Remote Sensing, IEEE Transactions on, vol. 44, pp. 694-706, 2006.
[8] C. Ruf and S. Misra, "Detection of Radio Frequency Interference with the Aquarius Radiometer," Geoscience and Remote Sensing Symposium, 2007. IGARSS 2007. IEEE International, pp. 2722-2725, 2007.
[9] B. Guner, J.T. Johnson and N. Niamsuwan, "Time and Frequency Blanking for Radio-Frequency Interference Mitigation in Microwave Radiometry," Geoscience and Remote Sensing, IEEE Transactions on, vol. 45, pp. 3672-3679, 2007.
[10] J.R. Piepmeier, P.N. Mohammed and J.J. Knuble, "A Double Detector for RFI Mitigation in Microwave Radiometers," Geoscience and Remote Sensing, IEEE Transactions on, vol. 46, pp. 458-465, 2008.
[11] R.D. De Roo, S. Misra and C.S. Ruf, "Sensitivity of the Kurtosis Statistic as a Detector of Pulsed Sinusoidal RFI," Geoscience and Remote Sensing, IEEE Transactions on, vol. 45, pp. 1938-1946, 2007.
[12] S.M. Kay, Fundamentals of Statistical Signal Processing: Detection Theory, volume 2, Prentice Hall: 1993, .